AIP | Review of Scientific Instruments

High-speed atomic force microscope combined with single-molecule fluorescence microscope

Shingo Fukuda, Takayuki Uchihashi, Ryota Iino, Yasutaka Okazaki, Masato Yoshida et al.

Citation: Rev. Sci. Instrum. **84**, 073706 (2013); doi: 10.1063/1.4813280
View online: http://dx.doi.org/10.1063/1.4813280
View Table of Contents: http://rsi.aip.org/resource/1/RSINAK/v84/i7
Published by the AIP Publishing LLC.

High-speed atomic force microscope combined with single-molecule fluorescence microscope

Shingo Fukuda,[1] Takayuki Uchihashi,[1,2] Ryota Iino,[3] Yasutaka Okazaki,[1] Masato Yoshida,[1] Kiyohiko Igarashi,[4] and Toshio Ando[1,2]
[1]*Department of Physics, College of Science and Engineering, Kanazawa University, Ishikawa 920-1192, Japan*
[2]*Bio-AFM Frontier Research Center, College of Science and Engineering, Kanazawa University, Ishikawa 920-1192, Japan*
[3]*Department of Applied Chemistry, School of Engineering, University of Tokyo, Tokyo 113-8656, Japan*
[4]*Department of Biomaterial Sciences, Graduate School of Agricultural and Life Sciences, University of Tokyo, Tokyo 113-8657, Japan*

(Received 22 April 2013; accepted 24 June 2013; published online 17 July 2013)

High-speed atomic force microscopy (HS-AFM) and total internal reflection fluorescence microscopy (TIRFM) have mutually complementary capabilities. Here, we report techniques to combine these microscopy systems so that both microscopy capabilities can be simultaneously used in the full extent. To combine the two systems, we have developed a tip-scan type HS-AFM instrument equipped with a device by which the laser beam from the optical lever detector can track the cantilever motion in the X- and Y-directions. This stand-alone HS-AFM system is mounted on an inverted optical microscope stage with a wide-area scanner. The capability of this combined system is demonstrated by simultaneous HS-AFM/TIRFM imaging of chitinase A moving on a chitin crystalline fiber and myosin V walking on an actin filament. © *2013 AIP Publishing LLC*. [http://dx.doi.org/10.1063/1.4813280]

I. INTRODUCTION

To increase the imaging rate of atomic force microscopy (AFM), elementary devices and control techniques were developed.[1–6] Moreover, a new feedback control technique was also developed to make the high-speed and low-invasive imaging capabilities compatible.[7] Through these developments, high-speed AFM (HS-AFM) has recently been established.[8,9] It permits direct imaging of biological molecules in action at high spatiotemporal resolution, without disturbing their functions. In fact, dynamically functioning proteins have been successfully visualized in succession; myosin V walking on an actin filament,[10] rotational propagation of conformational changes over three β subunits of rotorless F_1-ATPase,[11] bacteriorhodopsin responding to light,[12] cellulase moving unidirectionally during hydrolyzing a cellulose fiber,[13] and others.[14–17] The dynamic actions appeared in the molecular movies have provided great insights into the functional mechanisms of the proteins.[9] However, in-liquid AFM imaging, in general, has an intrinsic limitation as to the acquirable information. It is difficult to observe small chemicals such as ATP molecules. It is even impossible to visualize their binding to and dissociation from proteins, meaning that even when ligand-induce conformational changes of proteins are observed with HS-AFM, it is hard to directly verify that the observed changes are really induced by the binding or dissociation of small ligand molecules. Moreover, AFM is poor at identifying a specific target in a sample that contains multiple species of proteins, although efforts have been made to overcome this poorness.[18,19]

In contrast, fluorescence microscopy can easily detect fluorescence-emitting small molecules and identify one species of molecules in a sample containing multi-species of molecules. When fluorophores with different colors are used, it is even possible to identify two or three species of molecules in a sample with multiple components. Owing to these capabilities, fluorescence microscopy has been widely used in biological studies.[20–23] As a matter of course, fluorescence microscopy, however, cannot observe molecules that are not emitting fluorescence. Moreover, unlike AFM, it cannot resolve the structure of proteins.

As seen above, AFM and fluorescence microscopy are mutually complementary. Therefore, numerous developments of AFM combined with fluorescence microscopy have been made.[24–32] However, previous combined systems can perform neither optical imaging at the single molecule level nor fast AFM imaging. Here, we developed HS-AFM combined with objective lens type of total internal reflection fluorescence microscopy (TIRFM) with a capability of single-molecule imaging.[33] For the HS-AFM unit, we employed the tip-scan mode,[24] instead of the sample stage-scan mode, to make the full and simultaneous use of TIRFM possible. The HS-AFM unit is mounted on an inverted fluorescence microscope equipped with a slow, wide-area XY scanner on which a sample cell (or a cover slip) is placed. Here, we report the details of this instrumentation and demonstrate the capability of the combined system by simultaneous HS-AFM/TIRFM imaging of linear motions of proteins chitinase A and myosin V.

II. LASER-BEAM TRACKING

The current HS-AFM has employed the sample stage-scan mode.[8,9] Its high-speed performance, however, imposes restrictions on its application expansion. A large sample stage cannot be used, because it lowers the resonant frequencies of the scanner and hence the maximum possible imaging rate. In addition, the HS-AFM system is inadequate for making

simultaneous HS-AFM/fluorescence-microscopy observations possible, because the sample stage moves relative to the objective lens equipped for fluorescence microscopy. To eliminate these restrictions, we here developed a new HS-AFM system that operates in the tip-scan mode.

Designs for tip-scan AFM systems have been reported.[24,34–37] A common technical issue in the systems is the optical lever detection of cantilever deflection. The laser beam from the optical lever detector has to track the cantilever that is moving in the X- and Y-directions. HS-AFM uses small cantilevers and hence the size of a laser spot to be focused on a cantilever should be as small as the width of small cantilevers (~2 μm). Therefore, precise and fast laser-beam tracking is required for a tip-scan HS-AFM system. In typical tip-scan AFM systems previously developed, for example, by Werf *et al.*,[34] the laser diode and focusing lens are positioned inside the piezo tube and the cantilever is attached to the end of the piezo tube. This design is inadequate for HS-AFM, because an objective lens with a high numerical aperture (NA) has to be used to have a small laser spot on a small cantilever. Such an objective lens is too heavy to be scanned quickly. In another design developed by Nakano,[35] two mirrors, each being attached to either end of the Y-scanner, guide a laser beam to the cantilever and the laser beam reflected by the cantilever to the photodiode sensor. This method is only applicable to slow XY-scanners and not precise enough to be used for small cantilevers. Here, we use a laser beam tracking method that was previously used for Sagnac interferometry.[38] The tilt angles of a mirror placed in the optical path between the cantilever and the optical lever detector's photodiode sensor are scanned in synchrony with XY scanning of the cantilever. When the angle of the laser beam incident onto the objective lens is altered, the lateral position of the focused spot is displaced, as shown in Fig. 1(a). Figures 1(b) and 1(c) show the orthogonal side views of the two-dimensional mirror tilter that we developed here. The mirror tilter consists of two base plates, four piezo actuators (AE0203D04, NEC-TOKIN Corp., Miyagi, Japan) with the maximum displacement of ~3 μm at 100 V, and a dichroic mirror (NT64-464, >90% transmission at 400–690 nm, >95% reflection at 700–1150 nm, 12.5 × 12.5 mm^2, Edmond Optics, Barrington, NJ, USA). The dichroic mirror is supported by the X- and X′-piezoactuators, each of which is glued on the base plate 2 through a beveled block. This whole unit is supported by the Y- and Y′-piezoactuators that are glued on the base plate 1. The respective pairs of piezoactuators are displaced in the opposite directions, by which the respective tilt angles of the dichroic mirror are scanned. The base plates 1 and 2 have through-holes at their centers through which the cantilever and the focused laser spot can be viewed using a CCD camera, facilitating the adjustment of their relative position.

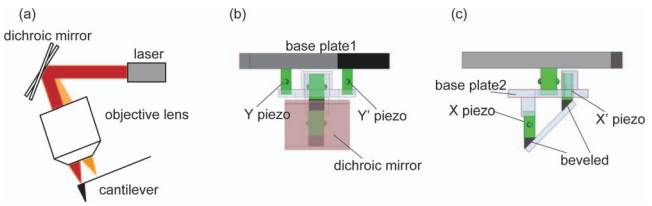

FIG. 1. Dichroic mirror tilter for laser-beam tracking of lateral cantilever motion. (a) Schematic showing the working principle of laser-beam tracking by mirror-tilting method. (b) and (c) Side views of the two-dimensional mirror tilter when viewed from two orthogonal directions.

From the maximum displacement of the piezoactuators and the size of the dichroic mirror, the maximum tilt-angle change $\pm\theta_{max}$ was estimated to be approximately $\pm 4.8 \times 10^{-4}$ rad for both tilters. The maximum displacement d_{max} of the focused laser spot is a function of the focal length (f_0 = 20 mm) of the ×20 objective lens (working distance, 24 mm; NA, 0.35; CFI L Plan EPI SLWD, Nikon, Tokyo, Japan) used for laser beam focusing as well as $\pm\theta_{max}$, which is approximately given by $d_{max} = 2f_o \times \theta_{max}$. This relationship gives d_{max} = 19 μm, which approximately agrees with an experimentally measured value, 20 μm.

The mirror tilting shifts the position where the laser beam reflected back by the cantilever is guided onto the two-segmented photodiode sensor. This shift produces a false cantilever deflection signal. However, this issue cannot be an impediment to tapping-mode HS-AFM which uses the cantilever oscillation amplitude to detect tip-sample interactions. This is because the cantilever oscillation frequency is much higher than the frequencies of mirror-tilter scanning, and because the amplitude signal is independent of the positional shift of the reflected laser beam at the photodiode sensor, which is much smaller than the diameter of the laser beam (~2 mm).

To assess the dichroic mirror tilter's dynamic performance, we have to directly measure the change in angle or displacement of a laser beam reflected back from the center of the dichroic mirror that is dynamically being tilted. However, it is difficult to do so. Instead, we measured the signal that is output from the optical lever sensor when the laser beam was reflected by the dichroic mirror and then by a stationary mirror and finally reflected by the dichroic mirror again. As the stationary mirror, the supporting base of a cantilever was used. Figure 2(a) shows frequency spectra of the signal that was output when the dichroic mirror was tilted by the X-and X′-piezoactuators (i.e., X-tilt). The first resonant peak appeared around 2.2 kHz, followed by a few peaks at higher frequencies. When the X-tilter is driven by an isosceles triangle wave, this mechanical response deteriorates the tracking and speed performance of the tilter, as shown in Fig. 2(b). This issue was solved by an inverse compensation method;[39] an isosceles triangle wave was digitally filtered by an inverse transfer function constructed using the frequency response shown in Fig. 2(a). Consequently, as shown by the red line in Fig. 2(c), the X-tilter moves smoothly approximately in an isosceles triangle wave, even when driven at 1 kHz, which corresponds to an imaging rate of 10 frames/s (fps) for 100 scan lines in the Y-direction. The red line in Fig. 2(c) is, however, slightly curved inwardly at the ascending regime and outwardly at the descending regime. This is not due to an effect of hysteresis of the piezoactuators used because such a nonlinear response does not appear when the X-tilter is scanned slowly. It is likely due to forced deformation of the dichroic mirror. This effect was eliminated by inverse compensation,[39] as shown by the orange line in Fig. 2(c).

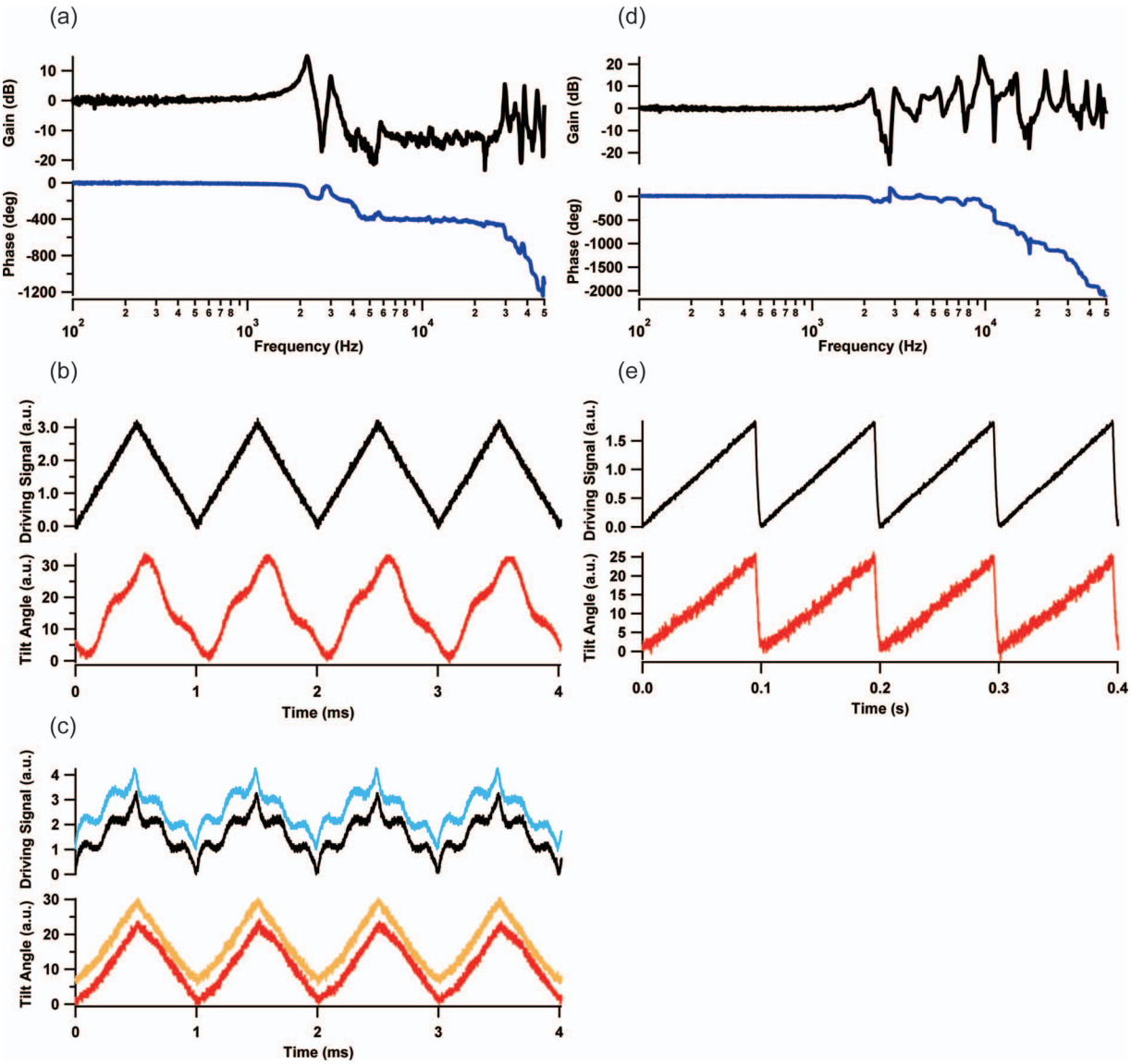

FIG. 2. Dynamic response of X- and Y-tilters. (a) Frequency spectra of tilting motion of the X-tilter (black line, gain; blue line, phase). (b) Tilting motion of X-tilter (red line) driven by 1 kHz isosceles triangle wave signal (black line). (c) Tilting motion of X-tilter (red line) driven by 1 kHz isosceles triangle signal filtered through inverse compensation (black line). The orange line shows the tilting motion when the filtered driving signal is further modified for the elimination of the curved response (blue line). (d) Frequency spectra of tilting motion of the Y-tilter (black line, gain; blue line, phase). (e) Tilting motion of Y-tilter (red line) driven by 10 Hz sawtooth wave signal (black line) whose precipitous downward part is slightly blunted.

To measure the dynamic performance of the Y-tilter, the two-segmented photodiode equipped with the optical lever sensor was rotated by 90°. The Y-tilter has the first resonant peak at 2.2 kHz and several larger peaks at higher frequencies, as shown in Fig. 2(d). Ideally, the tip scanner is scanned in the Y-direction in a sawtooth wave containing a precipitous downward regime, meaning that the Y-tilter should also be scanned in the same way. However, the precipitous scan for returning to the scan origin easily generates vibrations in both the tip-scanner and the dichroic-mirror tilter. We solved this problem by simply slowing the scanning to the scan origin. Even when slowed down, the time that this scan spends is much shorter than the time for which an image is captured. By this slower scanning to the scan origin, it was unnecessary to use inverse compensation in order to move the Y-tilter smoothly, as shown in Fig. 2(e).

Next, we evaluated the performance of the laser-beam tracking system by monitoring the amplitude of a small cantilever (BioLever fast BL-AC10DS-A2, Olympus; 9 μm long, 2 μm wide, and 130 nm thick; resonant frequencies 1.5 MHz in air and 600 kHz in water; spring constant ~0.1 N/m) which was freely oscillating during its scanning in the X- and Y-directions, without its tip being in contact with the sample surface. Figures 3(a) shows an amplitude image that was acquired at 1 fps without laser beam tracking when the cantilever tip oscillating in water at 600 kHz was scanned over a 650 × 650 nm^2 lateral area (256 × 256 pixels). The image contrast seen in Fig. 3(a) indicates that the optical lever sensitivity is changed by the positional shift of the cantilever relative to the laser spot focused on it. The height profile along the red line shown in Fig. 3(a) indicates that the apparent amplitude varies by ~1.4 nm_{p-p}, which is more than half the

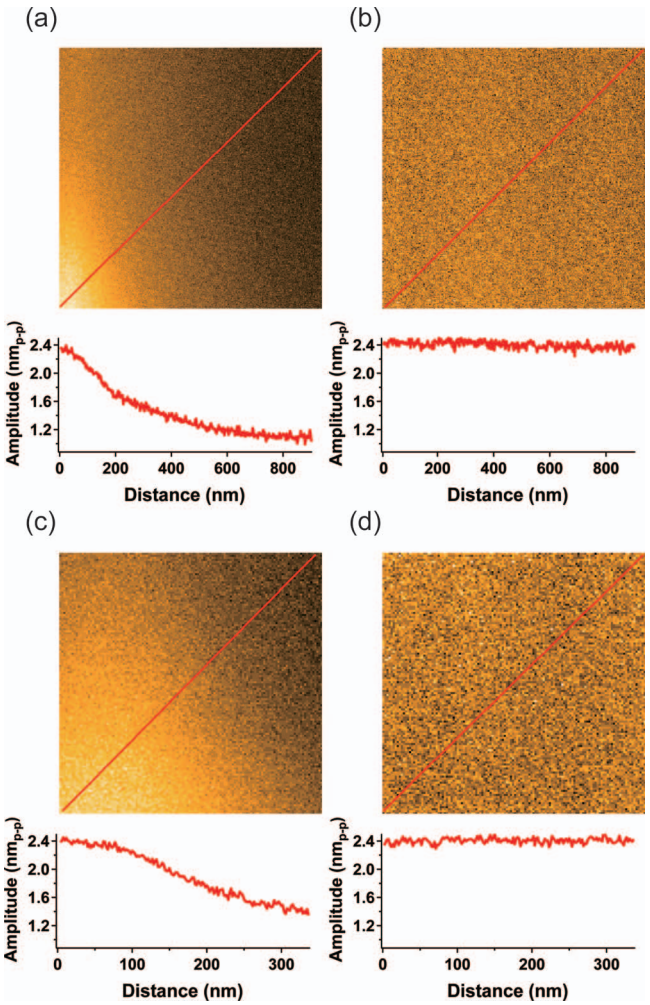

FIG. 3. Effect of laser-beam tracking of lateral cantilever motion on the optical lever detection of cantilever oscillation amplitude. (a) Amplitude image captured at 1 fps for 650 × 650 nm^2 (256 × 256 pixels) without laser-beam tracking. The bottom shows a height profile of the image along the diagonal red line. (b) Amplitude image captured at 1 fps for 650 × 650 nm^2 (256 × 256 pixels) with laser-beam tracking. The bottom shows a height profile of the image along the diagonal red line. (c) Amplitude image captured at 10 fps for 250 × 250 nm^2 (128 × 128 pixels) without laser-beam tracking. The bottom shows a height profile of the image along the diagonal red line. (d) Amplitude image captured at 10 fps for 250 × 250 nm^2 (128 × 128 pixels) with laser-beam tracking. The bottom shows a height profile of the image along the diagonal red line.

initial amplitude of 2.4 nm$_{p-p}$. Using the laser-beam tracking, this large error disappeared as shown in Fig. 3(b). The height profile along the red line shows the amplitude variation of only ∼0.2 nm, which mainly originates from thermal bending of the cantilever. Even when the imaging rate was increased to 10 fps for a smaller lateral area of 250 × 250 nm^2 (128 × 128 pixels), the tracking system worked well as shown in Fig. 3(d). The height variation was only ∼0.2 nm, making a large contrast with the large height variation that appeared when the tracking system was switched off [Fig. 3(c)]. Thus, the laser-beam tracking system can keep the optical lever's sensitivity of detecting cantilever oscillation amplitude constant, even when the cantilever tip is scanned at ∼1.3 kHz in the X-direction.

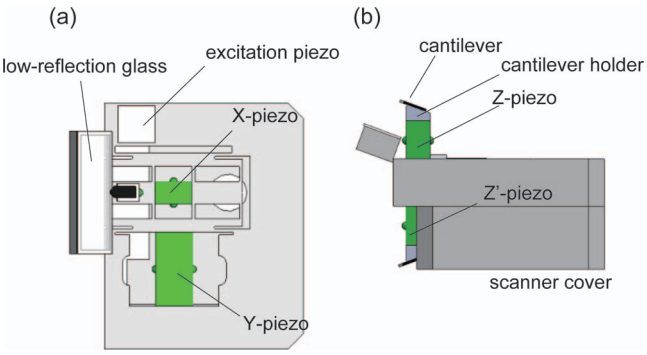

FIG. 4. Schematics of fast tip-scanner. (a) Bottom view. (b) Side view.

III. SCANNER

We developed a fast scanner for the tip-scan HS-AFM system, whose bottom and side views are shown in Figs. 4(a) and 4(b), respectively. Its design is basically the same as previously reported.[40] The piezoactuators used therein are AE0203D04 for X and AE0505D08 for Y, both from NEC Tokin Corp. (Miyagi, Japan). The X- and Y-scanners have the maximum displacements of 800 nm and 1.5 μm at 100 V and resonant frequencies of 18 kHz and 1.5 kHz, respectively. The mechanical vibrations produced by fast scanning of the X-scanner are suppressed by inverse compensation.[39] The Z-piezoactuator (AE0203D04) is glued on the block to be scanned in the X- and Y-directions. The electrodes protruding from the Z-piezoactuator are covered by a waterproof film as it is immersed in a buffer solution during AFM imaging. To maintain the Z-scanner's resonant frequency as high as possible, the cantilever holder to be attached to the Z-scanner is compact sized and made of silicon carbide that has a higher Young's modulus-to-density ratio than stainless steel and aluminum. The cantilever holder has a wedge shape with tip angle of 20° so that the cantilever held by it is tilted by this angle with respect to the sample substrate. The resonant frequency of the Z-scanner attached to the cantilever holder is 110 kHz and its maximum displacement is ∼3 μm at 100 V. As a counterbalance, an additional piezoactuator (Z′-piezoactuator) identical to the Z-piezoactuator is attached to the opposite face of the Z-scanner's supporting base. A dummy cantilever holder with a dummy cantilever is attached onto the Z′-piezoactuator. By this counterbalancing, the impulsive force generated by the rapid displacement of the Z-piezoactuator is counteracted with the impulsive force generated by the simultaneous displacement of the Z′-piezoactuator with the same velocity in the opposite direction.[1]

A piece of low-reflection glass (D263, Matsunami Glass Co. Ltd., Osaka, Japan) is placed just above the cantilever as an optical window for the laser beam, which can reduce reflection of the laser beam at the air-water interface. To acoustically excite the cantilever for tapping-mode operation, a thin piezoactuator (4.5Z4×4S-SYXC(C-82), Fuji Ceramics Co. Ltd., Shizuoka, Japan) with a resonant frequency of 2 MHz is placed on the scanner in proximity to the Z-piezoactuator.

IV. HS-AFM/TIRFM COMBINED SYSTEM

Figure 5(a) shows a schematic of the optical lever system for the tip-scan HS-AFM unit. Instead of a red laser used in the standard HS-AFM system,[8,9] an infrared (IR) laser (L980P010, $\lambda = 980$ nm, Thorlab, Newton, NJ, USA) is used because emission wavelengths of fluorescence dyes frequently used in fluorescence imaging are shorter than 800 nm. To suppress the optical feedback noise often caused by the laser beam that is reflected back or scattered back to the laser window, a radio-frequency laser power modulation is employed.[41] An objective lens with a long working distance ($\times$20, working distance 24 mm, NA 0.35, CFI L Plan EPI SLWD, Nikon, Tokyo, Japan) is used to focus the infrared laser onto the cantilever. The laser spot on the small cantilever can be observed with a CCD camera through the objective lens and the dichroic mirror, which facilitates the laser alignment. The cantilever deflection is detected by a position detection system consisting of a two-segmented Si PIN photodiode (S3096-02, Hamamatsu Photonics, Shizuoka, Japan), amplifiers, and a signal conditioner with total bandwidth of 20 MHz. Other optical components are optimized for the infrared wavelength: a collimation lens (LT110P-B, Thorlab, Newton, NJ, USA), a $\lambda/4$ wave-plate (WPQ-9800-4M, Sigma Koki, Tokyo, Japan), a polarization beam splitter (PBS103, Thorlab, Newton, NJ, USA), and a focusing lens (LA1074-B, Thorlab, Newton, NJ, USA) placed at the front of the two-segmented photodiode.

Figure 5(b) shows the side view of the newly designed tip-scan HS-AFM unit. The supporting frame of the unit is composed of top and base parts. Materials used for the top and base parts are aluminum and stainless steel, respectively. The center of gravity of the AFM unit is lowered as much as possible to make the unit robust to mechanical vibrations. All optical components for the optical lever system including the two-dimensional dichroic mirror tilter are assembled in the top frame. The fast scanner and a stepper motor (AM1020-2R-A-0.25-8-10+12/5 2050:1, Faulhaber GmbH, Weinheim, Germany) for the coarse tip approach are installed on the base part. The positions of the IR laser, the two-segmented photodiode, and the scanner with the cantilever can be adjusted with precise screws (F3ESK1, Thorlab, Newton, NJ, USA)

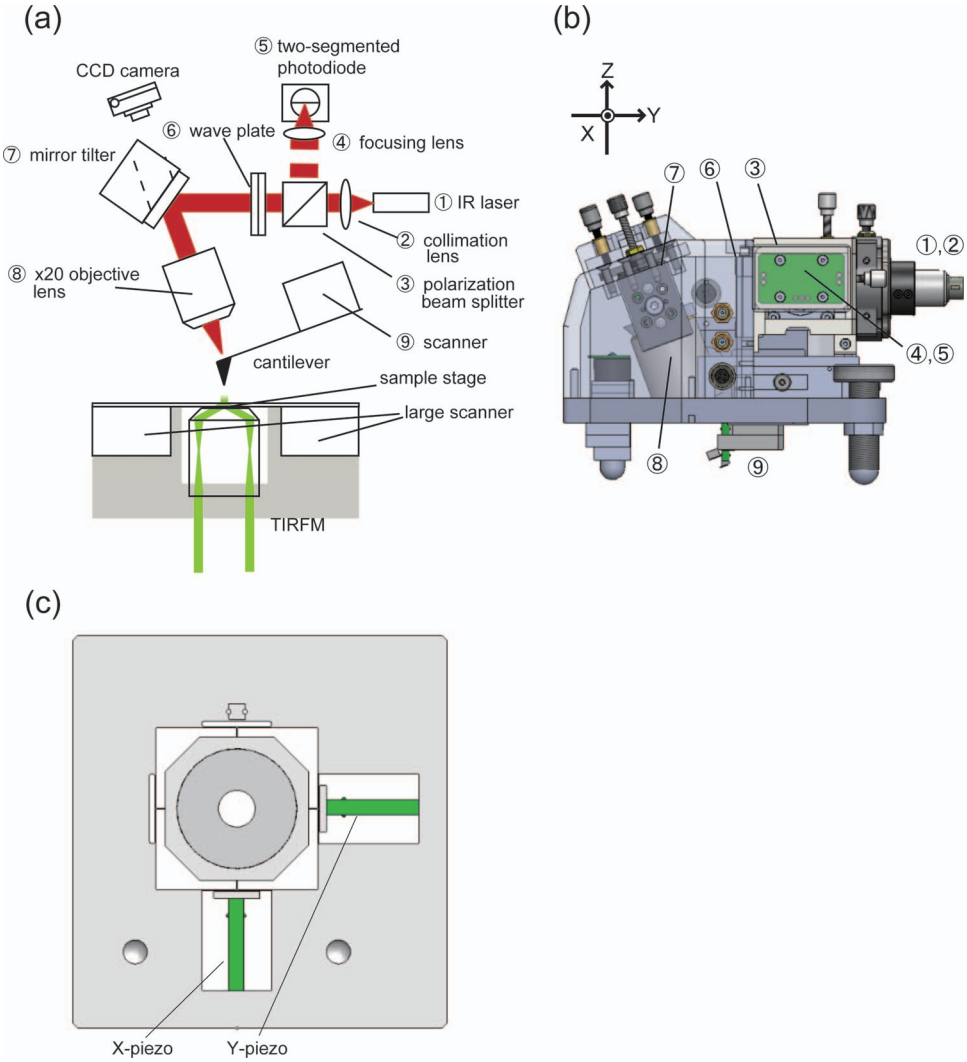

FIG. 5. Schematics showing the structure of tip-scan HS-AFM unit. (a) Optical lever detector with dichroic mirror tilter for laser-beam tracking. (b) Whole structure of the tip-scan HS-AFM unit. The numbers attached to respective parts correspond to the numbers shown in (a). (c) Optical microscope stage with wide-area XY-scanner.

in the XZ-, YZ-, and XY-planes, respectively, as shown in Fig. 5(b). The tilt angle of the dichroic mirror is also adjustable using three screws. The objective lens is also movable along its long axis for the adjustment of its focal point at the cantilever. The whole assembly is supported by a tripod consisting of two adjustable screws and a screw connected to the stepper motor. This tip-scan AFM unit is more compact than the standard HS-AFM head, facilitating its mounting on an optical microscope stage.

As an optical microscope to be combined with the tip-scan HS-AFM system, we used an inverted microscope (ECLIPSE Ti, Nikon, Tokyo, Japan) with modifications. In objective lens-based TIRFM, a high NA objective lens with a short working distance has to be used. The front face of the objective lens is usually in contact with a cover slip through immersion oil. In the standard configuration of inverted optical microscopes, the sample stage and objective lens are separately held within the microscope body. In this configuration, vibrations of the large microscope body are easily transmitted to the cover slip through the objective lens.[32] To minimize the mechanical coupling between the microscope body and the cover slip, the oil-immersion objective lens (Apo TIRF 100×, NA 1.49, Nikon, Tokyo, Japan) is directly hung from a custom-made microscope stage (Chukousya, Tokyo, Japan), instead of using the originally equipped objective lens revolver. In this microscope stage, the focus of the objective lens can be adjusted.

For video imaging by TIRFM, a relay lens (VM Lens C2.5X, Nikon, Tokyo, Japan) is connected to an EM CCD camera (Ixon3, Andor Technology, Belfast, Northern Ireland). The IR laser used in the HS-AFM's optical lever system is cut at the front of the CCD camera using an optical low-pass filter with 91% transmission at 400-810 nm and less than 0.01% transmission at 850–1190 nm (NT86-105, Edmond Optics, Barrington, NJ, USA).

The TIRFM setup has a wide field of view of ∼31 × 31 μm^2, whereas the maximum lateral scan range of the HS-AFM system is limited to 800 nm × 1.5 μm. This large difference makes it difficult to correlate acquired AFM images to TIRFM images. To fill this large gap, a wide-area XY-scanner is constructed in the optical microscope stage, using long-stroke piezoactuators (AE1010D44H40F, NEC Tokin Corp., Miyagi, Japan), as shown in Fig. 5(c). This wide-area scanner provides AFM images over a 15 × 15 μm^2 area, enabling precise positioning of the cantilever tip on the region of interest visualized by TIRFM. The Z-scanner in the HS-AFM unit is also used for slow AFM imaging performed using the wide-area XY-scanner.

V. SIMULTANEOUS HS-AFM/TIRFM IMAGING

First, we tested the performance of the tip-scan HS-AFM system by imaging tail-truncated myosin V (M5-HMM) molecules moving on actin filaments. As a sample substrate, cover slips (C030401, Matsunami Glass Co. Ltd., Osaka, Japan) were used. A circular area (7 mm in diameter) on a cover slip was surrounded by a Teflon sheet (965383, Niraco Co. Ltd, Tokyo. Japan) to avoid spreading of a buffer solution on the cover slip. Then, the cover slip surface

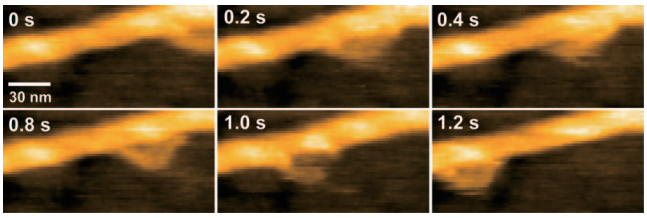

FIG. 6. Successive AFM images showing processive movement of M5-HMM along actin filament. The images were captured at 5 fps for an area of 150 × 75 nm^2 (100 × 40 pixels).

was coated with planar lipid bilayers using procedures similar to those used previously.[10,42] The lipid composition is 1,2-dipalmitoyl-sn-glycero-3-phosphocholine (DPPC), 1,2-dipalmitoyl-3-trimethylammonium-propane (DPTAP), and 1,2-dipalmitoyl-sn-glycero-3-phosphoethanolamine-*N*-(cap biotinyl) (biotin-cap-DPPE) in a weight ratio of 0.85:0.05:0.1. Partially biotinylated actin filaments were immobilized on the lipid bilayer surface through streptavidin with a low surface density. M5-HMM was injected to the 2 μM-ATP-containing buffer solution on the cover slip. Then, HS-AFM imaging was carried out at 5 fps for an area of 150 × 75 nm^2 (100 × 40 pixels). Figure 6 shows successive HS-AFM images of M5-HMM unidirectionally moving along an actin filament, from right to left. Thus, it was demonstrated that the tip-scan HS-AFM system developed here has an ability to capture protein molecules in action without disturbing their activity. However, the speed performance is somewhat inferior to the standard HS-AFM system because a piezoactuator used for the Z-scanner of the tip-scan HS-AFM has a longer working stroke (∼3 μm) than that used for the Z-scanner of the standard HS-AFM system (∼1 μm).

Figure 7(a) shows a TIRFM image of rhodamine-labeled actin filaments immobilized on a cover slip through avidin. After taking this image, positioning of the cantilever tip was made by reference to the TIRFM image, and then, HS-AFM

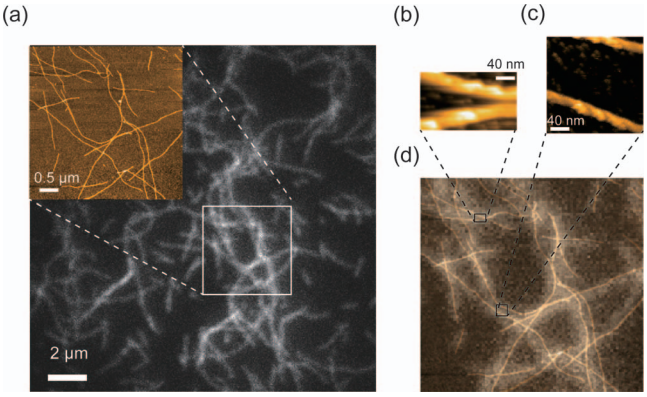

FIG. 7. Position-correlated TIRFM, AFM, and HS-AFM images of rhodamine-labeled actin filaments placed on a cover slip via avidin. (a) TIRFM image. The inset shows a wide-area AFM image captured at 10 min/frame for an area shown by the white rectangle in the TIRFM image. (b) HS-AFM image captured at 8.3 fps with 100 × 45 pixels. The position of cantilever tip was set by reference to the TIRFM image. (c) HS-AFM image captured at 2 fps with 100 × 100 pixels. The position of cantilever tip was set by reference to the TIRFM image. (d) The overlaid TIRFM/AFM images. The imaged areas of (b) and (c) are those shown by the black rectangles.

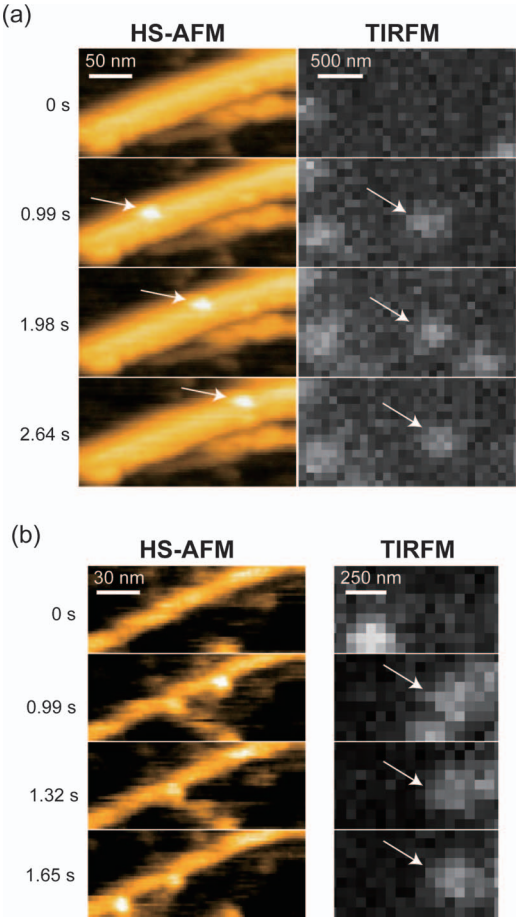

FIG. 8. Simultaneous HS-AFM/TIRFM imaging of proteins in action. (a) Cy3-labeled chitinase A on a chitin microfibril. The HS-AFM images (left) captured at 3 fps with 150 × 35 pixels show a single chitinase A molecule moving toward the top-right (arrows). The TIRFM images (right) with 40 × 15 pixels also show the same moving chitinase A molecule (arrows). (b) Cy3-labeled M5-HMM on an actin filament. The HS-AFM images (left) captured at 3 fps with 100 × 36 pixels^2 show a single M5-HMM molecule moving toward the bottom-left. The TIRFM images (right) with 17 × 9 pixels shows corresponding correlated fluorescent spots (white arrows) slightly moving from right to left.

imaging was carried out. The acquired HS-AFM images are shown in Figs. 7(b) and 7(c). However, it is difficult to find precise positional correlation between the TIRFM image and the HS-AFM images because individual actin filaments are not well resolved in the TIRFM image, particularly in the crowded area. However, wide-area AFM imaging with the use of the wide-area XY-scanner can solve this problem. The inset in Fig. 7(a) shows a wide-area AFM image taken by reference to the TIRFM image. This AFM image facilitates precise positional correlation between the TIRFM image and the HS-AFM images, as indicated in the overlaid TIRFM and AFM image shown in Figs. 7(d).

Finally, we tested the ability of our combined HS-AFM/TIRFM system to capture simultaneously the topographic and fluorescence images of single protein molecules in action. For the simultaneous recording, the synchronization between the two types of video recordings is required. For this synchronization, the exposure of the CCD camera was triggered at the beginning of each frame imaging by HS-AFM and the exposure time was adjusted to be slightly shorter than the frame time of HS-AFM. As test samples, we used chitinase A and M5-HMM, which are linear motor proteins. Chitinase A is known as an enzyme which degrades chitin microfibrils by hydrolysis and is considered to move processively and unidirectionally along the microfibrils.[43] For the fluorescence imaging, chitinase A was labeled with Cy3. Crystalline chitin microfibrils suspended in water were attached to a glass cover slip by spin coating. Figure 8(a) shows successive images of chitinase A moving along a chitin microfibril simultaneously observed by HS-AFM and TIRFM at an imaging rate of 3 fps. HS-AFM images (left) clearly shows binding of a single chitinase A molecule to the chitin microfibril at 0.99 s, as indicated by the white arrow. Then, the molecule moved with time on the microfibril toward the upper-right. A fluorescent spot appeared also at 0.99 s in the TIRFM images (right), as indicated by the white arrow. The fluorescent spot slightly moved with time toward the right side, although the movement is less conspicuous, because the field of view in the TIRFM is much wider than that of the HS-AFM.

Figure 8(b) shows simultaneously recorded HS-AFM and TIRFM images of a Cy3-labeled M5-HMM molecule bound to an actin filament in the presence of 3 μM ATP. Here, the glass surface was coated with lipid bilayers, as described above. The AFM images (left) show hand-over-hand movement of M5-HMM toward the bottom-left of the images. On the other hand, several fluorescent spots appeared in the TIRFM images (right). This is again because of the wide field of view in the TIRFM image. However, a fluorescent spot and a M5-HMM molecule appeared simultaneously in the TIRFM and HS-AFM images at 0.99 s, as indicated by the arrows. Thus, it was demonstrated here that the combined HS-AFM/TIRFM system can simultaneously capture respective images of the same biological molecules in action.

VI. CONCLUSION

We developed the combined HS-AFM/TIRFM system which can perform simultaneous topographic and fluorescence imaging at the single molecule level. The compact design of the HS-AFM unit with a laser-beam tracking capability allows its stand-alone operation and mounting on the inverted optical microscope stage. The slow but wide-area XY-scanner incorporated in the optical microscope stage fills the large gap in the field of view between HS-AFM and TIRFM, permitting precise finding of the positional correlation between their images. The tip-scan AFM can be operated at 5 fps, without disturbing the function of biological molecules. This speed performance is much better than conventional AFM systems but lower than the standard HS-AFM system. However, the speed performance can be improved when water-proof piezoactuators with a shorter working stroke are available. Moreover, since a fast wide-area scanner has recently been materialized,[44] the relatively narrow field of view in the tip-scan HS-AFM system can be improved in the near future, which will significantly expand the scope of HS-AFM/TIRFM system's application from

imaging of isolated biological molecules to imaging of dynamic events occurring in live cells.

The stand-alone configuration of the tip-scan HS-AFM unit permits its flexible use. We can combine the unit with different types of inverted optical microscopes: confocal microscopes and super-resolution fluorescence microscopes including stimulated emission depletion,[45] stochastic optical reconstruction,[46] and photo-activated localization[47] microscopes. Such ultra-hybrid microscopy systems will become powerful and innovative tools for biological science.

ACKNOWLEDGMENTS

This work was supported by Grant-in-Aid for Basic Research (Project ID 24227005 to T.A., 23115008 and 30326300 to T.U.), a JST's program on Development of Systems and Technology for Advanced Measurement and Analysis (to T.A.), HFSP (to T.A.), the Knowledge Cluster Initiative Project from the Ministry of Education, Culture, Sports, Science, and Technology Japan (to T.A.), and JST/ALCA (to T.U.).

[1]T. Ando, N. Kodera, E. Takai, D. Maruyama, K. Saito, and A. Toda, Proc. Natl. Acad. Sci. U.S.A. **98**, 12468 (2001).
[2]N. Kodera, H. Yamashita, and T. Ando, Rev. Sci. Instrum. **76**, 053708 (2005).
[3]T. Ando, T. Uchihashi, N. Kodera, A. Miyagi, R. Nakakita, H. Yamashita, and K. Matada, J. Surf. Sci. Nanotechnol. **3**, 384 (2005).
[4]M. B. Viani, T. E. Schäffer, G. T. Paloczi, L. I. Pietrasanta, B. L. Smith, J. B. Thompson, M. Richter, M. Rief, H. E. Gaub, K. W. Plaxco, A. N. Cleland, H. G. Hansma, and P. K. Hansma, Rev. Sci. Instrum. **70**, 4300 (1999).
[5]G. E. Fantner, P. Hegarty, J. H. Kindt, G. Schitter, G. A. G. Cidade, and P. K. Hansma, Rev. Sci. Instrum. **76**, 026118 (2005).
[6]G. Fantner, G. Schitter, J. H. Kindt, T. Ivanov, K. Ivanova, R. Patel, N. Holten-Andersen, J. Adams, P. J. Thurner, I. W. Rangelow, and P. K. Hansma, Ultramicroscopy **106**, 881 (2006).
[7]N. Kodera, M. Sakashita, and T. Ando, Rev. Sci. Instrum. **77**, 083704 (2006).
[8]T. Ando, T. Uchihashi, and T. Fukuma, Prog. Surf. Sci. **83**, 337 (2008).
[9]T. Ando, Nanotechnology **23**, 062001 (2012).
[10]N. Kodera, D. Yamamoto, R. Ishikawa, and T. Ando, Nature (London) **468**, 72 (2010).
[11]T. Uchihashi, R. Iino, T. Ando, and H. Noji, Science **333**, 755 (2011).
[12]M. Shibata, H. Yamashita, T. Uchihashi, H. Kandori, and T. Ando, Nat. Nanotechnol. **5**, 208 (2010).
[13]K. Igarashi, T. Uchihashi, A. Koivula, M. Wada, S. Kimura, T. Okamoto, M. Penttilä, T. Ando, and M. Samejima, Science **333**, 1279 (2011).
[14]M. Yokokawa, C. Wada, T. Ando, N. Sakai, A. Yagi, S. H. Yoshimura, and K. Takeyasu, EMBO J. **25**, 4567 (2006).
[15]D. Yamamoto, T. Uchihashi, N. Kodera, and T. Ando, Nanotechnology **19**, 384009 (2008).
[16]I. Casuso, J. Khao, M. Chami, P. Paul-Gilloteaux, M. Husain, J. P. Duneau, H. Stahlberg, J. N. Sturgis, and S. Scheuring, Nat. Nanotechnol. **7**, 525 (2012).
[17]A. Colom, I. Casuso, T. Boudier, and S. Scheuring, J. Mol. Biol. **423**, 249 (2012).
[18]C. Stroh, H. Wang, R. Bash, B. Ashcroft, J. Nelson, H. Gruber, D. Lohr, S. M. Lindsay, and P. Hinterdorfer, Proc. Natl. Acad. Sci. U.S.A. **101**, 12503 (2004).
[19]P. Hinterdorfer and Y. F. Dufrêne, Nat. Methods **3**, 347 (2006).
[20]Y. Sako and T. Yanagida, Nat. Rev. Mol. Cell Biol. **4**, SS1 (2003).
[21]C. Joo, H. Balci, Y. Ishitsuka, C. Buranachai, and T. Ha, Annu. Rev. Biochem. **77**, 51 (2008).
[22]H. Park, E. Toprak, and P. R. Selvin, Q. Rev. Biophys. **40**, 87 (2007).
[23]B. Huang, M. Bates, and X. Zhuang, Annu. Rev. Biochem. **78**, 993 (2009).
[24]C. A. J. Putman, H. G. Hansma, H. E. Gaub, and P. K. Hansma, Langmuir **8**, 3014 (1992).
[25]H. Nakajima, Y. Kunioka, K. Nakano, K. Shimizu, M. Seto, and T. Ando, Biochem. Biophys. Res. Commun. **234**, 178 (1997).
[26]J. Gorelik, A. Shevchuk, and M. Ramalho, Proc. Natl. Acad. Sci. U.S.A. **99**, 16018 (2002).
[27]A. B. Mathur, G. A. Truskey, and W. M. Reichert, Biophys. J. **78**, 1725 (2000).
[28]S. Nishida, Y. Funabashi, and A. Ikai, Ultramicroscopy **91**, 269 (2002).
[29]S. Hafizovic, D. Barrettino, T. Volden, J. Sedivy, K. Kirsten, O. Brand, and A. Hierlemann, Proc. Natl. Acad. Sci. U.S.A. **101**, 17011 (2004).
[30]R. Kassies, K. O. van der Werf, A. Lenferink, C. N. Hunter, J. D. Olsen, V. Subramaniam, and C. Otto, J. Microsc. **217**, 109 (2005).
[31]L. Peng, B. J. Stephens, K. Bonin, R. Cubicciotti, and M. Guthold, Microsc. Res. Tech. **70**, 372 (2007).
[32]H. Gumpp, S. W. Stahl, M. Strackharn, E. M. Puchner, and H. E. Gaub, Rev. Sci. Instrum. **80**, 063704 (2009).
[33]M. Tokunaga, K. Kitamura, K. Saito, A. H. Iwane, and T. Yanagida, Biochem. Biophys. Res. Commun. **235**, 47 (1997).
[34]K. O. van der Werf, C. A. J. Putman, B. G. de Grooth, F. B. Segerink, E. H. Schipper, N. F. van Hulst, and J. Greve, Rev. Sci. Instrum. **64**, 2892 (1993).
[35]K. Nakano, Rev. Sci. Instrum. **69**, 1406 (1998).
[36]M. Hipp, H. Bielefeldt, J. Colchero, O. Marti, and J. Mlynek, Ultramicroscopy **42–44**, 1498 (1992).
[37]C. Neagu, K. O. van der Werf, C. A. J. Putman, Y. M. Kraan, B. G. de Grooth, N. F. van Hulst, and J. Greve, J. Struct. Biol. **112**, 32 (1994).
[38]T. Tachizaki, T. Muroya, O. Matsuda, Y. Sugawara, D. H. Hurley, and O. B. Wright, Rev. Sci. Instrum. **77**, 043713 (2006).
[39]G. Schitter and A. Stemmer, IEEE Trans. Control Syst. Technol. **12**, 449 (2004).
[40]T. Ando, T. Uchihashi, and N. Kodera, Jpn. J. Appl. Phys. **51**, 08KA02 (2012).
[41]T. Fukuma, M. Kimura, K. Kobayashi, K. Matsushige, and H. Yamada, Rev. Sci. Instrum. **76**, 053704 (2005).
[42]D. Yamamoto, T. Uchihashi, N. Kodera, H. Yamashita, S. Nishikori, T. Ogura, M. Shibata, and T. Ando, Methods Enzymol. **475**, 541 (2010).
[43]T. Uchiyama, F. Katouno, N. Nikaidou, T. Nonaka, J. Sugiyama, and T. Watanabe, J. Biol. Chem. **276**, 41343 (2001).
[44]H. Watanabe, T. Uchihashi, T. Kobashi, M. Shibata, J. Nishiyama, R. Yasuda, and T. Ando, Rev. Sci. Instrum. **84**, 053702 (2013).
[45]K. I. Willig, S. O. Rizzoli, V. Westphal, R. Jahn, and S. W. Hell, Nature (London) **440**, 935 (2006).
[46]M. J. Rust, M. Bates, and X. W. Zhuang, Nat. Methods **3**, 793 (2006).
[47]E. Betzig, G. H. Patterson, R. Sougrat, O. W. Lindwasser, S. Olenych, J. S. Bonifacino, M. W. Davidson, J. Lippincott-Schwaetz, and H. F. Hess, Science **313**, 1642 (2006).